

Am Jang · Jeffrey Szabo · Ahmed A. Hosni ·
Michael Coughlin · Paul L. Bishop

Measurement of chlorine dioxide penetration in dairy process pipe biofilms during disinfection

Received: 13 September 2005 / Revised: 22 November 2005 / Accepted: 27 November 2005
© Springer-Verlag 2005

Abstract Biofilms are considered a significant health risk in the food and dairy industries because they can harbor pathogens, and direct contact with them can lead to food contamination. Biofilm control is often performed using strong oxidizing agents like chlorine and peracetic acid. Although chlorine dioxide (ClO₂) is being used increasingly to control microbiological growth in a number of different industries, not much is known about disinfection in biofilms using chlorine dioxide. In this study, a microelectrode originally made for chlorine detection was modified to measure the profiles of chlorine dioxide in biofilm as a function of depth into the biofilm. In addition, discarded microelectrodes proved useful for in situ direct measurement of biofilm thicknesses. The chlorine dioxide microelectrode had a linear response when calibrated up to a ClO₂ concentration of 0.4 mM. ClO₂ profiles showed depletion of disinfectant at 100 μm in the biofilm depth, indicating that ClO₂ may not reach bacteria in a biofilm thicker than this using a 25 mg/l solution.

Introduction

Biofouling may be defined as the attachment of biological materials to a solid surface that quickly form thin layers of microbial colonies. The microbial colonies, otherwise known as biofilms, constantly and rapidly develop a complex aggregation of microorganisms including bacteria, protozoa, amoebae, fungi, and algae, which are encased

in self-made extracellular polysaccharide. Biofouling commonly occurs in engineered systems, such as oil rigs, piping systems, drinking water distribution systems, heat exchangers, cooling towers, and ship hulls (De Beer et al. 1994; Meyer 2003). It causes equipment damage through corrosion, down time, and decreased energy efficiency due to the increased pressure drop in pipelines, which results in billions of dollars in losses each year (Meesters et al. 2003).

Food and dairy industries frequently encounter persistent biofouling problems that lead to solids buildup, spoilage, and bacterial contamination in pipes and process equipment. Fatemi and Frank (1999) described that biofilms developed on wet food-processing surfaces were not completely cleaned or not cleaned often enough. Michaels et al. (2001) reported that in the food industry, even under refrigerated conditions, pipeline biofilms could include spoilage microorganisms as well as pathogenic species. Recently, it has been reported that several *Bacillus cereus* strains associated with dairy products potentially cause food-borne illness as a result of toxin production (Lindsay et al. 2002). Therefore, process efficiency and safety in the food industry requires novel approaches to the prevention, removal, and killing of biofilms.

Biofilm control is often performed with strong oxidizing agents, of which the most commonly used is chlorine (Cl₂). Although gaseous chlorine has long been used as a simple and economic method for disinfection, its use as a microbicide is declining because of safety, environment, and community impact considerations. Furthermore, it has been found that chlorination may form disinfection by-products (DBPs) such as trihalomethanes (THMs) and haloacetic acids (HAAs), by oxidizing organic matter (fulvic and humic acids) in water. It is well documented that these products are harmful to consumers' health (Junli et al. 1997; Chang et al. 2001). As a result of these concerns, various alternatives have been explored, including peracetic acid, chloramine, ozone, and chlorine dioxide (ClO₂) (Lopez et al. 1997; Fatemi and Frank 1999; Richardson et al. 2000; Chang et al. 2001). As one of the promising disinfectants, chlorine dioxide has become more widespread as it offers some unique advantages, including

A. Jang · J. Szabo · A. A. Hosni · P. L. Bishop (✉)
Department of Civil and Environmental Engineering,
University of Cincinnati,
Cincinnati, OH 45221-0071, USA
e-mail: Paul.Bishop@UC.edu
Tel.: +1-513-5563675
Fax: +1-513-5563930

M. Coughlin
JohnsonDiversey, Incorporated Innovation Center,
3630 East Kemper Road,
Cincinnati, OH 45241, USA

its easy operation and maintenance, requirement for a smaller dosage, less reaction time to yield same disinfection effect as Cl_2 , and effectiveness over a wide pH range on killing bacteria or deactivating virus (Chang et al. 2000). Some water systems have started treating tap water with ClO_2 as a substitute for Cl_2 as ClO_2 does not directly form halogenated by-products (Noss and Olivieri 1985).

It is generally accepted that disinfectants are much less effective against biofilm microorganisms than planktonic microorganisms (De Beer et al. 1994; Cochran et al. 2000). Although the fundamental mechanisms of biofilm resistance have not been fully elucidated (Stewart and Raquepas 1995), this is fundamentally due to the chemical reaction of the disinfectants with extracellular polymeric substance (EPS) and other organic constituents that form the biofilm. Furthermore, disinfectants may not reach bacteria deep in the biofilm as a result of diffusional resistance of the biofilm matrix, which may exist even after disinfection.

The objective of this study was an investigation of the efficacy of ClO_2 as a disinfectant by measuring ClO_2 penetration into simulated dairy biofilms. Concentration profiles of ClO_2 in biofilms can be achieved with high spatial resolution by the use of microelectrodes. These tiny, needle-shaped electrochemical sensors have a tip diameter of around $10\ \mu\text{m}$, which prevents disruption of the biofilm during the measurement of concentration profiles.

Materials and methods

Operation of the rotating drum biofilm annular reactor (RDBAR)

The design and operation of a continuous aerobic rotating drum biofilm annular reactor (RDBAR), as shown in Fig. 1, was previously described by Zhang (1994). Briefly, the reactor consists of a concentric outer cylinder (inner diameter of 11.7 cm) and a rotating inner cylinder with a total height of 25.4 cm. The acrylic reactor, with a 1-l working volume, was designed for continuous-flow operation. The inner cylinder was rotated at 90 rpm and completely mixed the fluid in the reactor. Temperature was maintained at $23\pm 0.5^\circ\text{C}$. The reactor contained 40 removable 304 stainless steel coupons on its inner wall to permit sampling of the biofilms. New stainless steel was cut into 1-cm^2 coupons. Coupons were cleaned once in acetone and rinsed with deionized water prior to installation in the reactor.

Biofilm was grown in the RDBAR using a mixed culture of undefined consortia from unpasteurized whole milk by the following procedure. The RDBAR was seeded with unpasteurized whole milk and operated in batch mode for 1 day. The reactor was then drained and refilled with sterile 10% trypticase soy broth (TSB) and operated in continuous flow mode for the duration of the experiment. Sterile 10% TSB was pumped through the reactor at a flow rate of 0.6 l/h, resulting in a hydraulic retention time (HRT) of 2 h. Biofilm on the stainless steel coupon surfaces became visible after 7 days of growth. Biofilm samples were

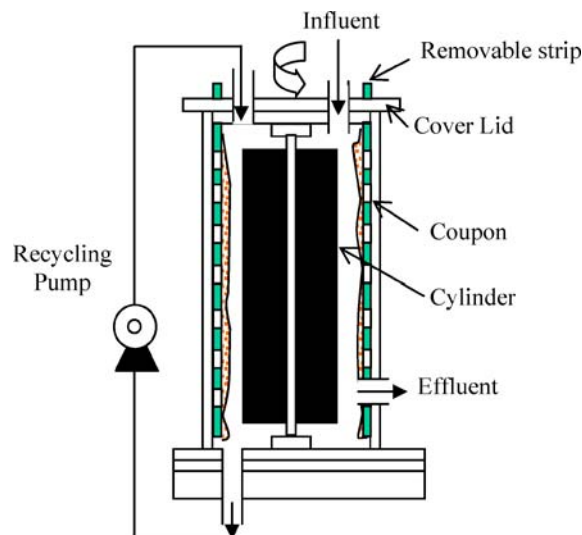


Fig. 1 Schematic diagram of rotating drum biofilm annular reactor (RDBAR) used in this study (reactor working volume, 1000 ml, reactor height and diameter, 25.4 and 11.7 cm; flow rate, 0.6 l/hr; HRT, 2 h; temperature, $23\pm 0.5^\circ\text{C}$; impeller peripheral velocity, 90 rpm)

removed at specific time intervals after the reactor was seeded to analyze disinfection performance at various biofilm thicknesses.

Microelectrode fabrication

The microelectrode assembly was as described by De Beer et al. (1994) and Yu (2000), except that an operating potential of 100 mV was used for chlorine dioxide instead of the 200 mV that DeBeer et al. used for chlorine. The signal for chlorine dioxide was found to be better at 100 mV. Briefly, the cathode was made from platinum wire (Aldrich, Milwaukee, WI, USA, No. 26,716-3, purity 99.99%) melted into a lead glass micropipette (World Precision Instruments, Sarasota, FL, USA, No. PG10150-4). The wire was etched in 6 M potassium cyanide (KCN) by applying a 5-V potential while continuously dipping the wire into the solution; the platinum wire was attached to a graphite reference electrode. Micropipettes were heated over the flame of a small burner until the glass softened. They were pulled from both ends until the middle section of the micropipette became very fine but still unbroken. The platinum wire was very carefully inserted into the hollow center of the pulled glass micropipette at one end until the etched tip of the platinum wire reached the fine middle section of the micropipette. The center of the micropipette (containing the etched platinum tip) was placed in a heating element. This element melted and sealed the glass around the wire tip. The voltage was slowly increased during the heating operation, resulting in even sealing. Increasing the heat sharply before the tip reaches the heating element prevents the platinum wire from breaking off before reaching the tip. Next, the platinum tip was exposed by beveling, and the glass was

resealed by reheating the tip for approximately 2 s in the heating element. Subsequently, the platinum in the tip was recessed approximately 1 to 2 μm using fresh 2 M KCN solution while applying 2.5 V of alternating current. The etched platinum wire was then cleaned by immersing it sequentially in three beakers of distilled water. The whole process of etching must be conducted in a highly ventilated hood to prevent inhalation of cyanide gas. Finally, a cellulose acetate coating was applied by submerging the tip in a 10% acetone solution for 30 s. The coating dried for 1 h at room temperature. The tip diameters of the resulting microelectrodes were 7 to 15 μm .

Microelectrode measurements

During calibration and concentration measurements, 0.1 V was applied to the chlorine dioxide and reference electrodes. The pico-ampere current signal was measured with a chemical microsensor (Model II, Diamond General, Ann Arbor, MI, USA). Biofilm samples were placed in a specially designed flow cell inside a Faraday cage to minimize electrical interferences. The whole system was connected to a scrupulously clean-grounded line. Positioning the tip of the microelectrode in the biofilm was accomplished using a three-dimension micromanipulator (Model 11N, Narishige International, Tokyo, Japan) located outside the Faraday cage. The position relative to the biofilm surface was determined visually using a microscope, CCD camera, and video monitor. Because of irregularities, biofilm surfaces are not always well defined. The surface of the biofilm was located by recording when the microelectrode tip visually disappeared as it approached the biofilm. The flow rate of the solution into the flow cell was maintained at 10 ml/min as previous studies have shown that flows of 50 ml/min or more would interfere with the microelectrode measurements by creating signal noise (Zhang and Bishop 1994). A peristaltic pump was used to achieve the necessary flow above the biofilm. Chlorine dioxide concentration profiles, from the bulk in a direction perpendicular to the biofilm surface, were measured at 5, 10 and 15 min after exposure. The bulk solution concentration was 25 mg/l. An Ag/AgCl millielectrode was used as the reference electrode for all working microelectrodes throughout the study. More than five microelectrode profiles were measured at different positions along the biofilm axis during the investigation. The tip of the microelectrode was rinsed in distilled water between each experiment change.

Microscopic examination of cross-sectioned biofilms

Coupons and attached biofilm were removed from the reactor, dipped into 1 ml of 4% paraformaldehyde and stored at 4°C overnight. The coupons and attached biofilm were then washed with 1×PBS buffer solution, embedded in tissue-freezing compound, and then immediately frozen at -20°C for cryosectioning. The solidified biofilm was

fixed on a specimen stage of a cryostatic microtome (HM 505E, Microm International GmbH, Germany). Biofilm samples were cut vertical to the coupon surface into 20- μm -thick slices using a steel razor blade and spread on a gelatin-coated slide. The slide was then immersed into serial 50, 80, and 95% ethanol solutions for 3 min each and dried. Biofilms on the slide were observed using a microscope (Nikon) under $\times 400$ magnification.

Preparation of ClO_2

Sachets of sodium chlorite (NaClO_2 , Selective Micro Technologies, Beverly, MA, USA) were supplied by JohnsonDiversey. The sodium chlorite within the sachet was activated by filling it with 2 l of distilled water, which provided a solution containing approximately 120 mg ClO_2/l . The ClO_2 solution, which is very volatile and unstable, was placed in a dark brown glass container and stored in the dark at 4°C. The concentration of the ClO_2 solution was directly measured using a DR/2010 spectrophotometer (Hach Method 10126, HACH Company, Loveland, CO, USA) just before application. This is a standard *N,N*-diethyl-*p*-phenylenediamine (DPD) color change method described by Standard Methods for the Examination of Water and Wastewater (2005) (4500- ClO_2 D). In addition, the ClO_2 concentration in the flow cell was measured regularly during the experimentation with the DR/2010 spectrophotometer. The results were comparable to those obtained using the ClO_2 microelectrode.

Results

ClO_2 microelectrode

When both the ClO_2 microelectrode and the Ag/AgCl reference electrode are immersed in ClO_2 solution, the ClO_2 diffuses to the cathode where ClO_2 is reduced to chloride ions. Silver is oxidized to silver chloride at the anode at the same time. The current resulting from this reaction is a direct measurement of the concentration of the ClO_2 in solution. A Faraday cage was used to isolate the ClO_2 microelectrode from external electrical noise. However, it was found that the current signals varied from one microelectrode to another, depending on the geometry of the working electrode (i.e., electrode surface area and recess length). The stability of ClO_2 microelectrodes with tip diameters of 10 μm was checked using a standard pH 7 buffer solution. When 0.1 V was imposed on the working and reference electrodes, the signal in the blank was in the range of 50–100 pA. If the current in the blank solution was lower or higher than this range, the microelectrode was discarded. Response time of the ClO_2 microelectrode to reach 90% of the final stable reading was less than 1–2 s. Furthermore, drift of the reduction current was usually below 1% per hour.

After checking the stability of the ClO_2 microelectrodes, they were calibrated with a ClO_2 calibration series (0 to

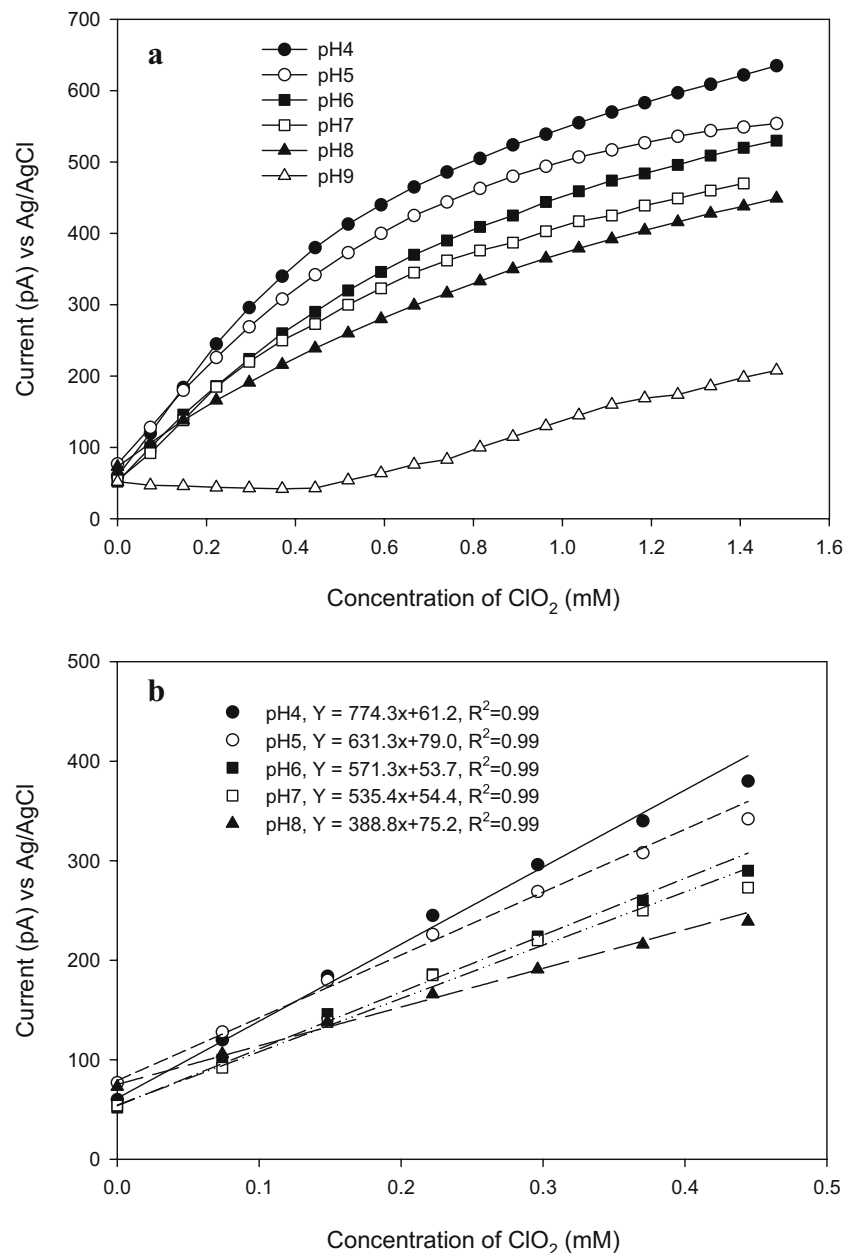
1.48 mM) in standard pH buffer solutions of pH 4, 5, 7, 8, and 9. Three measurements were made and the average picoampere current was used to determine the calibration sensitivity for ClO₂. The results from the effects of initial pH on the ClO₂ microelectrode calibration curve show two stages of slope. In the beginning, the signal increase was linearly proportional to increasing ClO₂ concentration in contact with the platinum (Pt) surface of the microelectrode. At greater than 0.44 mM, however, a nonlinear signal response was observed.

The results in Fig. 2a show that the signal increases varied, some with pH up to pH 8, with the response decreasing only slightly with increase in pH at lower ClO₂ concentrations. However, the trends observed for the currents measured at pH 9 were different from those in

the range of pH 4–8. It is assumed that the ClO₂ microelectrode is significantly affected by changes at pH 9, possibly due to an increase of the ratio of [NaClO₂] to [ClO₂] in the solution. This may be one reason for the reduced signal observed at pH 9. As the biofilm reactors were operated at pH 7, the profiles measured in this study were conducted at the same pH.

When the ClO₂ microelectrode was calibrated up to a concentration of 0.44 mM, as shown in Fig. 2b, there is a linear proportionality between current measured and ClO₂ concentration in the ranges of pH 4–8. The ClO₂ concentration range of 0–0.44 mM lies well within the linear part of the curve and is well suited for monitoring most biofilms. Although slightly different slopes (pA/mM) of the calibration curves are observed depending on the initial

Fig. 2 a Signal variability at different pH and ClO₂ bulk concentrations. b The calibration curve of a ClO₂ microelectrode at various pH values



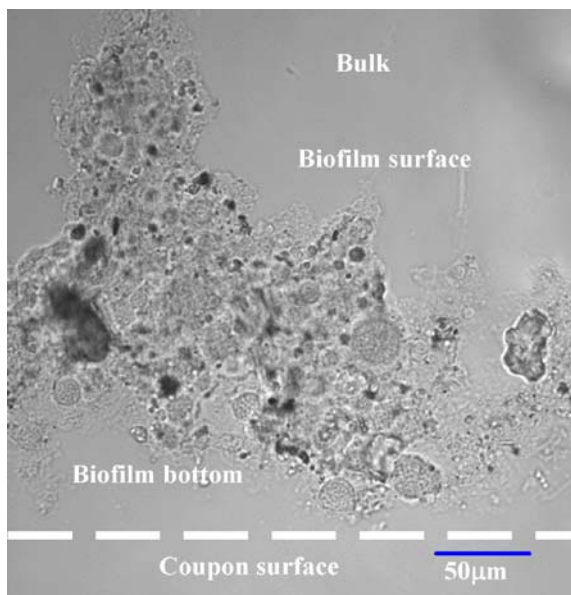


Fig. 3 A microscopic image of the spatial biofilm section attached to the surface of a stainless steel coupon. The biofilm sample was cut vertical to the coupon into 20- μm -thick slices using a cryostatic microtome. The *scale bar* shown on the figure is 50 μm

pH, reasonable linear curve fits were obtained. During all measurements of ClO_2 concentration in biofilm, the flow rate of the solution was maintained to be under 10 ml/min.

ClO_2 penetration depth

Biofilm thickness, as shown in Fig. 3, was visualized by light microscopy. The biofilm seemed smooth when observed with the naked eye, but numerous heterogeneities appeared when viewed under the microscope. Biofilm

thickness varied spatially on the coupon but usually fell between 150 and 200 μm .

Figure 4 shows the ClO_2 microprofiles in a biofilm obtained when using a ClO_2 microelectrode and a bulk liquid concentration of 25 mg ClO_2/l adjusted to pH 7. Profiles were measured at 5, 10, and 15 min after the start of the chlorine dioxide dosing at the same position in the biofilm. All ClO_2 profiles showed similar trends, although the actual concentration of ClO_2 measured in a single biofilm varied slightly, depending on the sampling location. The sigmoidal shapes of the ClO_2 microprofiles show that, in the cases of 5 and 10 min after the start of the chlorine dioxide dosing, ClO_2 was depleted at a depth of 50 μm . After 15 min, however, the shape of the ClO_2 profiles had slightly changed. The inflection point of the concentration profile moved in the direction of the coupon, and the penetration depth of ClO_2 in the biofilm was increased to approximately 100 μm . This may be due to changes in the ClO_2 demand in the upper layers of the biofilm due to oxidation of organic matter by ClO_2 .

The chlorine dioxide concentration continued to decrease in the 150- μm -thick mass transfer diffusion boundary layer above the surface of the biofilm. From the nearly linear gradient within the mass transfer boundary layer, it is evident that the diffusion layer governs the rate of exchange of substrate between the bulk liquid and the biofilm. Consequently, the existence of a boundary layer cannot be ignored in a mathematical model interpretation. The profiles of ClO_2 showed a trend of gradual decrease from the biofilm surface toward the coupon surface, which is characteristic for ClO_2 that is diffusing into a matrix where it is being consumed.

An experiment to examine if multiple punctures of the biofilm might boost its permeability was carried out. A profile in the biofilm was measured and the tip was then removed from the biofilm. The tip was then immediately

Fig. 4 Concentration microprofiles of ClO_2 in biofilm at a bulk ClO_2 concentration of 25 mg/l. The profiles were measured 5, 10, and 15 min after the start of the ClO_2 dosing at the same points in the same biofilm. Point 0 on the x-axis indicates the biofilm surface. Positive depth values (to the *right* of 0) are in the bulk, and negative depth values (*left* of zero) are in the biofilm

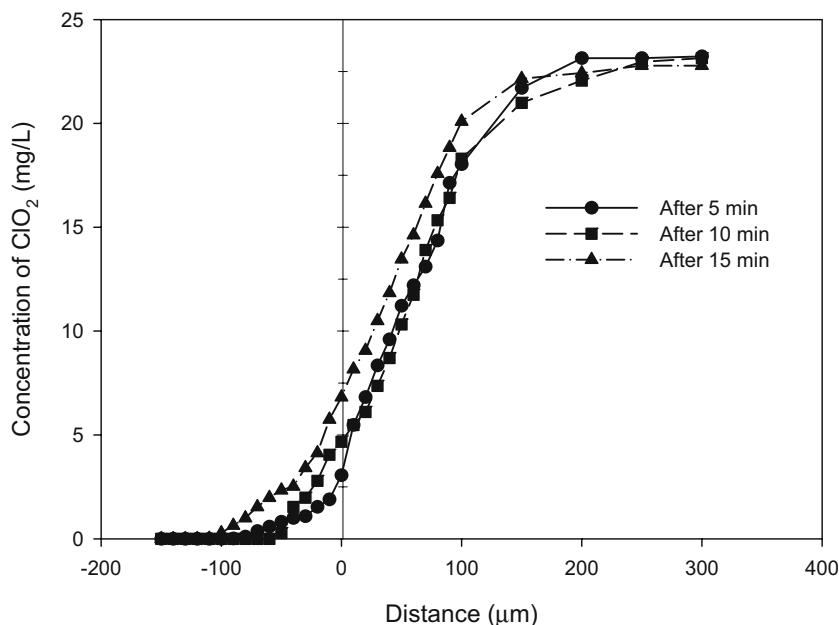
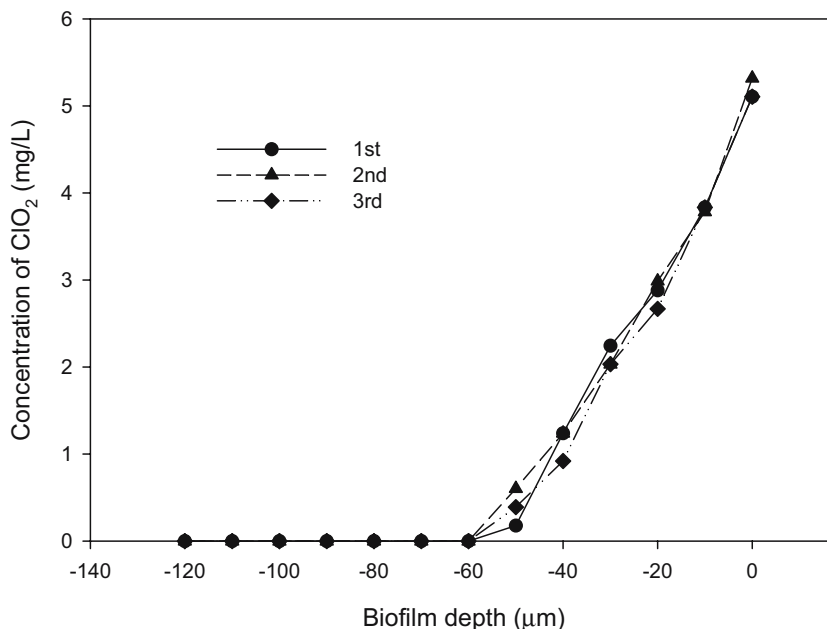


Fig. 5 Concentration microprofile of ClO_2 at a single point



reinserted at the same location and the profile was measured again. The tip was removed again and the process repeated a third time. As shown in Fig. 5, the same concentration profile was measured for three consecutive times when the microelectrode was removed and reinserted. This shows that permeability does not increase as the biofilm is punctured (at least for microelectrodes with tips of 10–15 μm like what we used).

Parameter estimation for mathematical modeling

Mathematical modeling can analyze chlorine dioxide consumption kinetics. Due to the high diversity and complexity of biofilms, some simplifications concerning

the reactions that take place in the biofilm are necessary for development of biofilm models where antimicrobial agents such as ClO_2 are involved. The assumptions used in this study are described elsewhere (Lu et al. 1995; Stewart and Raquepas 1995). Models such as those described hereafter are useful because they predict qualitative phenomena and suggest new experimental designs. Parameter determination methods used for full model development are described elsewhere (Abrahamson et al. 1996).

As observed in Fig. 4, chlorine dioxide transport from the bulk solution to the biofilm decreased both near the diffusive boundary layer and in the biofilm, probably due to the mass transfer resistance, leading to the development of the substrate concentration gradient. It is assumed that transport in the stagnant liquid layer above the substrate is

Fig. 6 Determination of experimental constant A

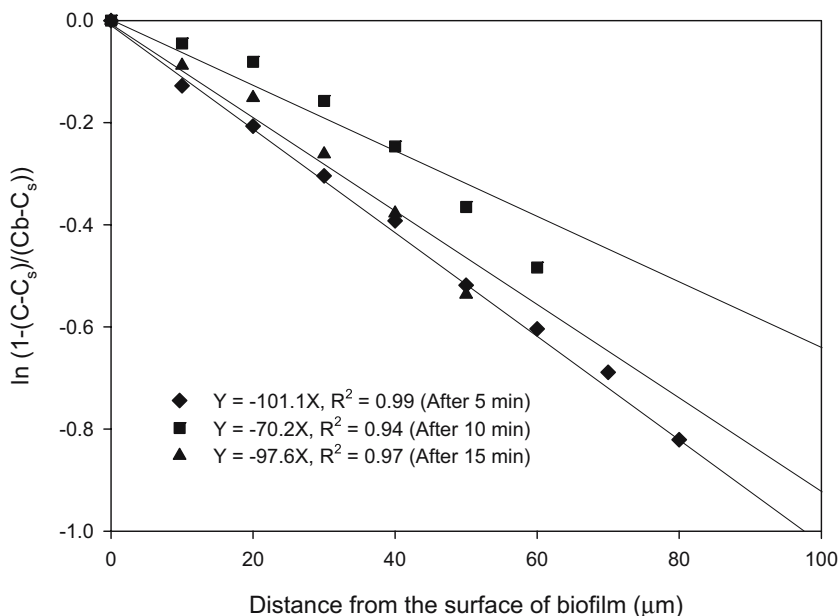
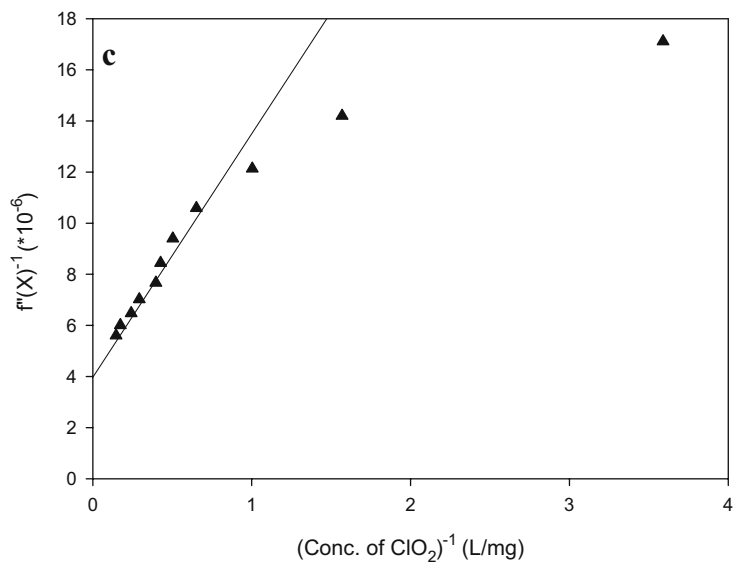
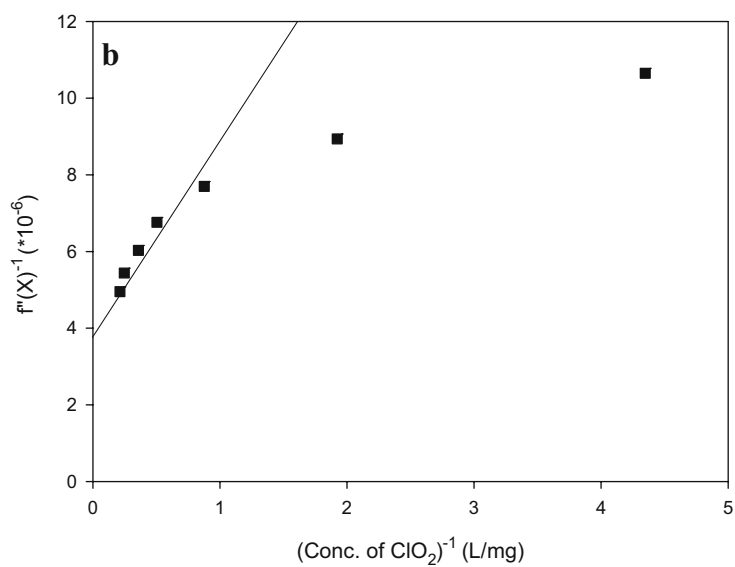
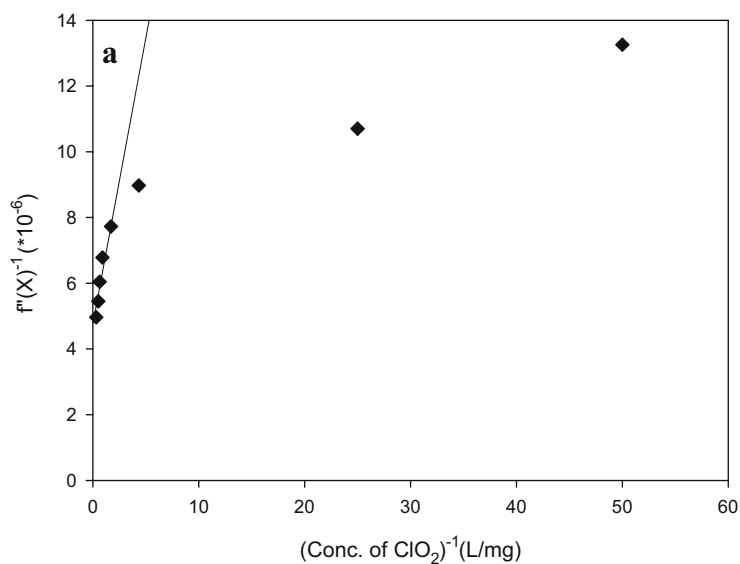


Fig. 7 Lineweaver–Burk plot for determination of half-saturation constant: **a** after 5 min, **b** after 10 min, and **c** after 15 min



entirely dependent on molecular diffusion, which can be described by Fick's first law (Abrahamson et al. 1996). This assumption yields the following empirical linearized Eq. (1):

$$\frac{C - C_s}{C_b - C_s} = 1 - \exp(-Az) \quad (1)$$

where C is the local ClO_2 concentration, C_s is the ClO_2 concentration at the surface of the biofilm, C_b is the ClO_2 concentration in the bulk, A is an experimental constant determined graphically from the slope of Eq. (1), and z is the vertical distance into the biofilm. Figure 6 shows an example of the plot for the determination of A . At 5, 10, and 15 min after the start of the chlorine dioxide dosing at a given position within the biofilm, the slopes in Fig. 6 were 101.1, 70.2, and 97.6, respectively.

For the study of microbial activity in the biofilm, the classical transient diffusion–reaction model can be obtained from a mass balance in the biofilm. As written in Eq. (2), the chlorine dioxide consumption at any point in the biofilm per unit volume of biofilm attached to the coupon, as the chlorine dioxide penetrates the biofilm, is expressed by the Monod equation.

$$\frac{\partial C}{\partial t} = D_f \frac{\partial^2 C}{\partial Z^2} - \frac{V_{\max} C}{K_m + C} \quad (2)$$

At steady-state,

$$D_f = \left(\frac{\partial^2 C}{\partial Z^2} \right)_f = \frac{V_{\max} C}{K_m + C} \quad (3)$$

where subscript f represents biofilm, t is the time, D_f is an average effective diffusion coefficient of ClO_2 in the biofilm, Z is the distance into the biofilm from the biofilm surface, V_{\max} is the maximum ClO_2 utilization rate, and K_m is the Monod saturation constant. The parameters to be estimated in Eq. (3) are the kinetics parameters (V_{\max} and K_m) and ClO_2 diffusivity (D_f). A mathematical process is necessary to find the values of these parameters. According to Lineweaver–Burk linearization, Eq. (3) can be linearized by taking the inverse of each part in Eq. (3).

$$\left(\frac{d^2 C}{dZ^2} \right)_f^{-1} = \frac{D_f K_m}{V_{\max}} \frac{1}{C} + \frac{D_f}{V_{\max}} \quad (4)$$

The relationship between $(d^2 C/dZ^2)^{-1}$ and $1/C$ is illustrated in Fig. 7. A plot of $(d^2 C/dZ^2)^{-1}$ vs $1/C$ should result in a straight line with a slope of $D_f K_m/V_{\max}$ and an ordinate intercept of D_f/V_{\max} . Consequently, K_m can be calculated from the slope and the intercept of the line. As shown in Fig. 7, a good curve fit is obtained if high $1/C$ values (low concentration) are neglected. Therefore, the lower concentration limit for linearity is about 1.0 mg/l. By

plotting Eq. (4) within the acceptable range of the low $1/C$ values, the values of K_m calculated from the slope divided by the intercept of the straight line for 5, 10, and 15 min after the start of the chlorine dioxide dosing are 0.4, 1.0, and 1.6 mg/l, respectively.

After integrating Eq. (3) once, the ClO_2 transport flux rate ($\text{g/m}^2/\text{day}$) into a unit area of a biofilm can be obtained as (Lewandowski et al. 1991):

$$\begin{aligned} J_f &= D_f \left(\frac{dC}{dZ} \right)_f \\ &= D_f \sqrt{2 \frac{V_{\max}}{D_f} \left(C - C_0 - K_m \ln \frac{K_m + C}{K_m + C_0} \right)} \end{aligned} \quad (5)$$

From Eq. (5) and as seen in Fig. 4, the ClO_2 concentration in the biofilm near the surface of the substratum (C_0) is nearly zero. At a low bulk liquid ClO_2 concentration, the equation that depicts the ClO_2 concentration near the biofilm surface is

$$\left(\frac{dC}{dZ} \right)_{f|(Z=Z_s)} = \sqrt{2 \frac{V_{\max}}{D_f} \left(C_s - K_m \ln \frac{K_m + C_s}{K_m} \right)} \quad (6)$$

It was reported that at steady-state, the consumption rate is equal to the diffusion rate inside the biofilm (Hibiya et al. 2004). Therefore, it can be assumed that the flux rate of ClO_2 consumption inside the microbial film (J_f) is equal to the ClO_2 flux across the stagnant layer (J_w).

$$\begin{aligned} J_{f|(Z=Z_s)} &= J_{w|(Z=Z_s)}, \text{ or } D_f \left(\frac{dC}{dZ} \right)_{f|(Z=Z_s)} \\ &= D_w \left(\frac{dC}{dZ} \right)_{w|(Z=Z_s)} \end{aligned} \quad (7)$$

To calculate the internal effective diffusivity (D_f) in the biofilm, the terms on the right side of Eq. (7) can be divided by the second term on its left side. The ClO_2 diffusivity (D_w) in water is $1.385 \times 10^{-5} \text{ cm}^2/\text{s}$ at 20°C (Lide 2004). Moreover, the first derivative in the boundary layer can be expressed as follows:

$$\left(\frac{dC}{dZ} \right)_{w|(Z=Z_s)} = -A(C_b - C_s) \quad (8)$$

The effective diffusivity of ClO_2 in the biofilm was calculated to be 1.21×10^{-5} , 1.27×10^{-5} , and $1.35 \times 10^{-5} \text{ cm}^2/\text{s}$ for 5, 10, and 15 min after the start of the chlorine dioxide dosing, respectively, showing that the effective diffusion coefficients of ClO_2 in biofilms were reduced somewhat from their values in the bulk solution.

Discussion

The food and dairy industries are frequently plagued by microbial contamination in pipes and process equipment. Biofilm formation in the food service environment causes not only economic losses due to technical failure in process equipment but can also lead to significant hygiene problems; the biofilm can harbor pathogens, and direct contact with them can lead to food contamination. Although chlorine dioxide is being used increasingly to control microbiological growth in a number of different industries, not much is known about disinfection in biofilms using chlorine dioxide. Chlorine dioxide profiles in the biofilm were obtained using microelectrodes modified from an existing design.

Chlorine dioxide may not reach bacteria deep in a biofilm as a result of multiple resistance factors, such as molecular diffusion limitations, biofilm density, reactive depletion of ClO_2 , and convective flow rate in interstitial voids. One of the primary factors suggested by many researchers is transport limitation of antimicrobial agents into the biofilm community (Xu et al. 1998). Although the primary mechanism, interaction of ClO_2 with the biofilm has not been fully examined, the EPS produced by microorganisms in the biofilm may partially protect them from the disinfectant properties of the ClO_2 . Inactivation and/or removal of bacteria deep in the biofilm, consequently, may need to be achieved by increasing the concentration of ClO_2 in the bulk liquid and/or by increased contact time.

Although microscopic images provide valuable information with regard to biofilm structure, this method was highly time and labor intensive. As an alternative, discarded ClO_2 microelectrodes with intact tips could be used to provide a quick estimate of biofilm thickness. A light source was placed over the top of the biofilm, and then the microelectrode tip was positioned at the biofilm surface. The tip of the ClO_2 microelectrode was then slowly moved through the biofilm. When the ClO_2 microelectrode touched the surface of the stainless steel coupon, the shaft of the ClO_2 microelectrode bent without breaking. This bend could be easily identified from observation of the microelectrode shaft above the surface of the biofilm. Depth was calculated by determining the starting and ending positions of the micromanipulator. Normally, about 10–15 thickness measurements were taken in situ at random locations on each coupon. This method was simple and reasonably accurate for measuring the biofilm depth.

Acknowledgement This research was supported by a contract from JohnsonDiversey, Inc., Cincinnati, OH.

References

- Abrahamson M, Lewandowski Z, Geesey G, Skjåk-Bræk G, Strand W, Christensen BE (1996) Development of an artificial biofilm to study the effects of a single microcolony on mass transport. *J Microbiol Methods* 26(1–2):161–169
- Chang C-Y, Hsieh Y-H, Shih I-C, Hsu S-S, Wang K-H (2000) The formation and control of disinfection by-products using chlorine dioxide. *Chemosphere* 41:1181–1186
- Chang C-Y, Hsieh Y-H, Lin Y-M, Hu P-Y, Liu C-C, Wang K-H (2001) The organic precursors affecting the formation of disinfection by-products with chlorine dioxide. *Chemosphere* 44:1153–1158
- Cochran WL, McFeters GA, Stewart PS (2000) Reduced susceptibility of thin *Pseudomonas aeruginosa* biofilms to hydrogen peroxide and monochloramine. *J Appl Microbiol* 88(1):22–30
- De Beer D, Srinivasan R, Stewart PS (1994) Direct measurement of chlorine penetration into biofilms during disinfection. *Appl Environ Microbiol* 60:4339–4344
- Eaton A, Clesceri L, Greenberg A (eds) (2005) Standard methods for the examination of water and wastewater, 21st edn. American Public Health Association, Washington, DC
- Fatemi P, Frank, JF (1999) Inactivation of *Listeria monocytogenes*/*Pseudomonas* biofilms by peracid sanitizers. *J Food Prot* 62:761–765
- Hibiya K, Nagai J, Tsuneda S, Hirata A (2004) Simple prediction of oxygen penetration depth in biofilms for wastewater treatment. *Biochem Eng J* 19(1):61–68
- Junli H, Li W, Nanqi R, Fang M, Juli (1997) Disinfection effect of chlorine dioxide on bacteria in water. *Water Res* 31(3):607–613
- Lewandowski Z, Walser G, Characklis G (1991) Reaction kinetics in biofilms. *Biotechnol Bioeng* 38:877–882
- Lide DR (2004) CRC Handbook of chemistry and physics, 84th edn. CRC, Boca Raton, FL
- Lindsay D, Brözel VS, Mostert JF, von Holy A (2002) Differential efficacy of a chlorine dioxide-containing sanitizer against single species and binary biofilms of a dairy-associated *Bacillus cereus* and a *Pseudomonas fluorescens* isolate. *J Appl Microbiol* 92(2):352–361
- Lopez A, Mascolo G, Tiravanti G, Passino R (1997) Degradation of herbicides (ametryn and isoproturon) during water disinfection by means of two oxidants (hypochlorite and chlorine dioxide). *Water Sci Technol* 35(4):129–136
- Lu C, Biswas P, Clark RM (1995) Simultaneous transport of substrate, disinfectants and microorganisms in water pipes. *Water Res* 29(3):881–894
- Meesters KPH, Van Groenestijn JW, Gerritse J (2003) Biofouling reduction in recalculating cooling systems through biofiltration of process water. *Water Res* 37:525–532
- Meyer B (2003) Approaches to prevention, removal and killing of biofilms. *Int Biodeterior Biodegrad* 51:249–253
- Michaels B, Ayers T, Celis M, Gangar V (2001) Inactivation of refrigerator biofilm bacteria for application in the food service environment. *Food Service Technology* 1:169–179
- Norwood DE, Gilmour A (2000) The growth and resistance to sodium hypochlorite of *Listeria monocytogenes* in a steady-state multispecies biofilm. *J Appl Microbiol* 88:512–520
- Noss CI, Olivieri, VP (1985) Disinfecting capabilities of oxychlorine compounds. *Appl Environ Microbiol* 50:1162–1164
- Richardson SD Jr, Thruston AD, Caughran TV, Chen PH, Collette T, Schenck KM Jr, Lykins BW, Rav-Acha C, Glezer V (2000) Identification of new drinking water disinfection byproducts from ozone, chlorine dioxide, chloramine, and chlorine. *Water Air Soil Pollut* 123:95–102
- Stewart, PS, Raquepas JB (1995) Implications of reaction–diffusion theory for the disinfection of microbial biofilms by reactive antimicrobial agents. *Chem Eng Sci* 50(19):3099–3104
- Xu KD, Stewart PS, Xia F, Huang CT, Mcfeters GA (1998) Spatial physiological heterogeneity in *Pseudomonas aeruginosa* biofilm is determined by oxygen availability. *Appl Environ Microbiol* 64(10):4035–4039
- Yu T (2000) Stratification of microbial processes and redox potential changes in biofilms. Dissertation. University of Cincinnati, Cincinnati, Ohio, USA
- Zhang TC (1994) Influence of biofilm structure on transport and transformation processes in biofilms. Dissertation, University of Cincinnati, Cincinnati, Ohio, USA
- Zhang TC, Bishop PL (1994) Density, porosity and pore structure of biofilms. *Water Res* 28:2267–2277